A Comparative Study of Different Approaches to Modeling the Solar Wind

Sun, X. and Hoeksema, J. T.

W.W. Hansen Experimental Physics Laboratory (HEPL), Stanford University

Abstract:

The Wang-Sheeley-Arge (WSA) model is regularly used to predict the background solar wind speed and the interplanetary magnetic field (IMF) polarity from photospheric observation. The predictions near the sun are made from an empirical formula which has two parameters: (1) the magnetic expansion factor and (2) the minimum angular distance from a field line foot point to the edge of the coronal hole. A kinetic propagation model is then used to determine the values at 1AU. In this paper, we address that two factors can affect the result to a significant extent: (1) treatment of input data and (2) the algorithm used to compute the two parameters. We study the model dependence of the prediction and try to optimize the method with different approaches. Three different models (potential field source surface (PFSS) model, Schatten current sheet (SCS) model integrated with PFSS, and horizontal-current current-sheet source-surface (HCCSSS) model) are discussed here. The predictions perform variously in different phases of the solar cycle, with SCS generally gives a better prediction.

Introduction

The solar wind speed is closely connected with the coronal fields. Assuming materials are transported along the flux tubes, WSA uses two parameters from the modeled coronal field to predict the solar wind speed.

1. Flux tube expansion factor (f_s): for a flux tube connecting a certain height R and the photosphere:

$$f_s = \frac{B_{photo}}{B}\frac{R_{photo}^2}{R^2}.$$

Wang (1990) shows that there's an inverse relation between the observed solar wind speed and the expansion factor, which means the more flux tube expands, the slower the solar wind is.

2. Angular distance from the foot points to the nearest coronal hole boundary θ_b. This parameter

distinguishes the high speed solar winds from the low speed ones. High speed wind that comes from the center of a coronal hole has large θ_b; low speed wind that comes from the hole boundary has a small θ_b. The introduction of this new parameter greatly improves the accuracy of prediction.

An empirical function, with various free parameters in the following form (Arge, 2003), is used to predict the solar wind speed near the sun (fig1).

$$v = 265 + \frac{1.5}{(1+f_s)^{0.4}}[5.8 - 1.5\exp(1-(\frac{\theta_b}{2.5})^{2.0})]^{3.5}.$$

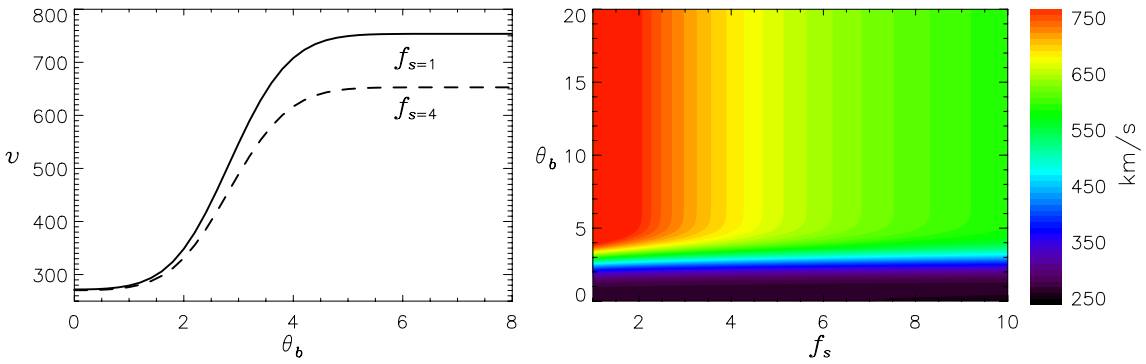

Fig1 Left: Solar wind speed as a function of θ_b, for fixed f_s

Right: Contour of speed in the (f_s, θ_b) space given by the empirical function.

The two parameters can be obtained from any coronal field models. Since we are more interested in the global structures, simple models are preferred here. In this study, we explore three existing models: PFSS, SCS and HCCSSS (fig2). All three models start from the simple potential field assumption:

$$\nabla \cdot \vec{B} = 0,$$

with the effects of various currents being included later.

1. PFSS: Potential Field Source Surface Model
   - Potential field everywhere
   - Fields become open and purely radial from a certain height (source surface)
2. SCS: Schatten Current Sheet Model
   - Potential field below the source surface where fields become open and radial
   - Current sheet exists above the source surface, where field is realigned
   - No radial field confinement above the source surface
3. HCCSSS: Horizontal-Current Current-Sheet Source-Surface Model
   - Source surface placed near the Alfvén critical point, where all the fields become radial

- Introduces cusp surface, where field becomes open but not necessarily radial. Include effects of streamer current sheets.
- Horizontal electric current in the lower corona is included as a free parameter.

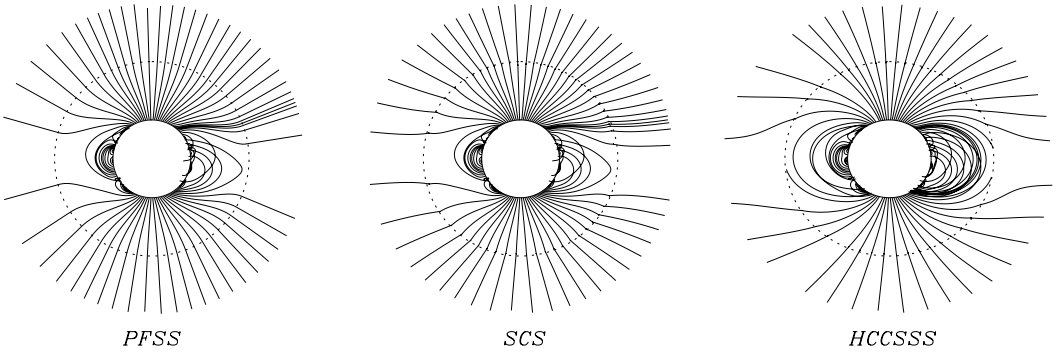

Fig2 Derived field configuration from three models (CR1922, MDI data).

The disk center has a Carrington longitude of 240º. The dashed circle implies a $2.5R_{\odot}$ sphere.

The PFSS model requires the field to be radial at source surface. Although no current is allowed below this surface, the hidden assumption of this radial constraint suggests a horizontal volume current in the higher corona. It is most successful in reproducing structures in lower corona. The original current sheet model (PFCS), which also has a purely potential field in the lower corona but includes the current sheet higher up, does not require the field to be radial at the source surface. It is most successful in predicting open field structures such as polar plumes and the axes of coronal streamers. The HCCSSS model introduces a horizontal current everywhere and relaxes the radial field requirement at $2.5R_{\odot}$ as to satisfy the solution of magneto-static equation (Low, 1985), so the field becomes more smooth on the interface and fits observation best among the three (Zhao and Hoeksema, 1995).

The current version of current sheet model (SCS), which runs routinely at NOAA, has an additional radial confinement on the source surface. In this way, the lower coronal structures could be described more accurately. But there is also one drawback: the tangential field clearly becomes discontinuous at the source surface.

While extensive work has been done to incorporate the PFSS and SCS model into the WSA model, little has been explored for the HCCSSS model. The coronal model dependence of the prediction is unknown either. In this study, we try to follow the existing procedures and explore various possible improvements.

Data Processing and Computation Scheme:

Observed photospheric field is used as the only input of the model. For a high resolution MDI line of sight (LOS) synoptic chart (3600x1080 in sine latitude), several procedures are essential:

1. Correct for the effect of the solar *b* angle and convert LOS map into a radial field map.
2. Convert the map to a lower resolution of 2.5º (144x72), from sine latitude to latitude, with flux conserved both locally and globally.
3. Use well observed polar field data and a temporal interpolation (Liu, 2007) to fill in the polar regions.
4. Remove the monopole.

Using one of the three models, we trace the field line downward from a certain height ($2.5R_\odot$ for PFSS, $5R_\odot$ for SCS and HCCSSS) to the photosphere. If we assume the solar wind materials are transported along the flux tube from a lower height, then those field lines can specify the source of the solar winds.

The two parameters are then computed near the sun. We use a simple 1D kinetic model to propagate the solar wind from the sub-earth points to 1AU. Materials travel radially. When faster solar winds catch up with the slower ones, they interact and obtain a new speed. This way, we get the time series of solar wind speed 1AU with a 4 hour resolution.

As a validation of this method, 4-hour averaged WIND data is used. We crosscheck the WIND proton speed data with OMNI proton temperature, remove the points with extra low proton temperature, which is an indicator of CMEs (Richardson, 1995). Mean square error (MSE) is used to evaluate the predictions and to optimize the empirical function.

Field Configuration from Three Models:

After tracing the field lines down, we map the foot points on the photosphere and the neutral lines on the cusp/source surface. For all three models, over the solar cycle, inferred neutral lines based on MDI data are generally consistent with those from WSO data and PFSS model (fig3). The difference mainly results from the polar field correction, where a north-south asymmetry is sometimes introduced. As we will demonstrate later, a proper polar field is crucial for a correct prediction. Except for solar maximum, the derived foot points locations are generally consistent with Kitt Peak and EIT data.

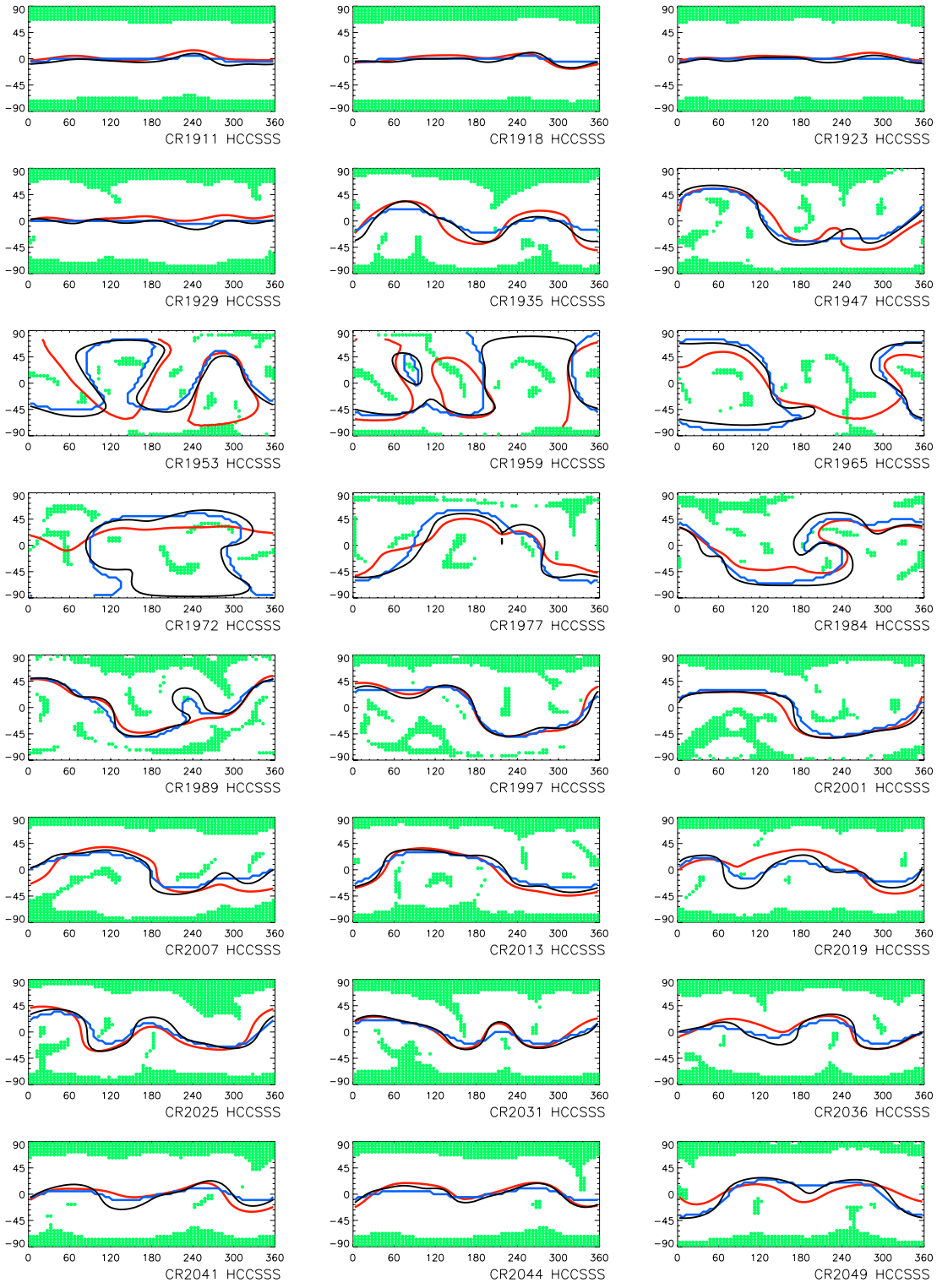

Fig3 Foot points and neutral line map from HCCSSS. (MDI, order 9)

Green areas: open field foot points; Black line: derived cusp surface (2.5$R_\odot$) neutral line;

Blue line: source surface (15$R_\odot$) neutral line; Red line: neutral line from WSO website, based on PFSS model.

Because of the introduced currents, neutral lines at $5R_\odot$ (SCS) are usually flatter than the PFSS model, and those at $15R_\odot$ of HCCSSS flatter than the SCS model. For SCS and HCCSSS model, neutral lines at different heights ($2.5R_\odot$ and $5R_\odot$ for SCS; $2.5R_\odot$ and $15R_\odot$ for HCCSSS) are nearly identical. This indicates that fields are nearly radial near the current sheet, between these two heights, though they are not required to be so.

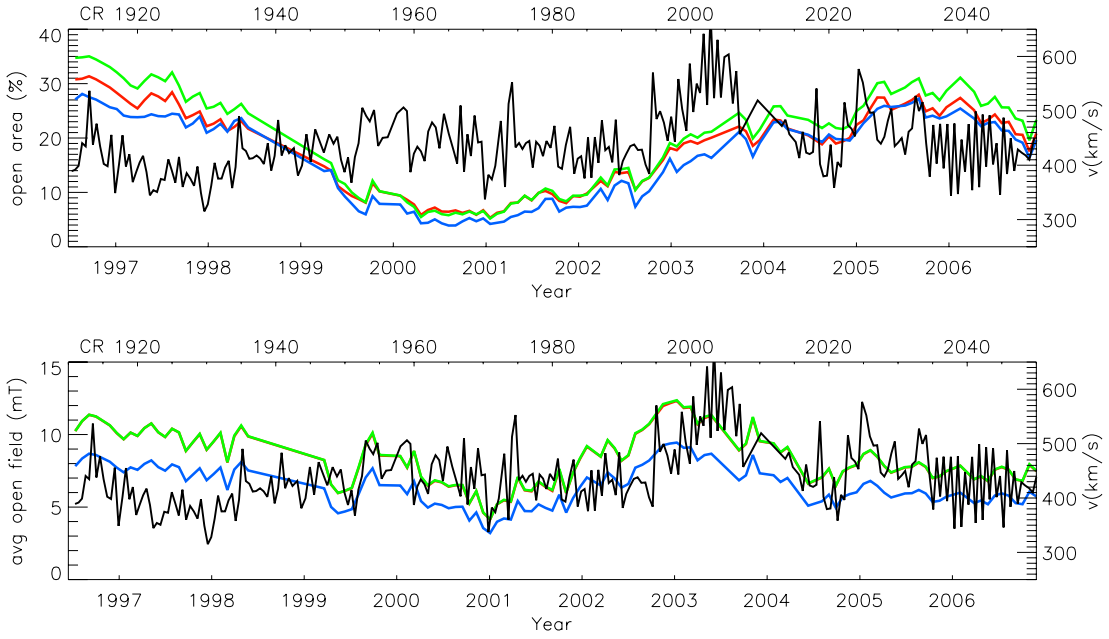

Fig4 Upper: Open flux region area derived from three models. (MDI, od22). Lower: average absolute B_r

Red: PFSS; Green: SCS; Blue: HCCSSS; Black: solar wind speed from WIND

The area of the open flux region at solar surface and the total absolute flux at $2.5R_\odot$ vary during the solar cycle. The results derived from different models are significantly different, too. Amongst the three models, SCS gives an open flux region 21% larger and a total absolute flux 31% greater than HCCSSS (fig4). The difference in the field configuration mainly comes from the radial constraint at $2.5R_\odot$, as different choice of horizontal current and height of source surface in HCCSSS won't change the field configuration below $2.5R_\odot$. Without this radial confinement, polar field flux tubes tend to extend to lower latitude instead of opening up at higher latitude, which results a greater expanded polar field and a somewhat strong low latitude field. As we trace the field lines on a even grid from a certain height in HCCSSS, more go back to the higher latitude, thus results in smaller open flux regions and absolute fluxes. This feature determines the performance of solar wind speed prediction based on HCCSSS model.

For comparison, we lower the starting height of tracing for HCCSSS to $5R_{\odot}$ in the following work. This doesn't change the nature of the result since the fields are mostly radial above this height, as we mentioned above.

Comparison of Predictions: CR1922 and CR1987

Carrington rotation 1922 (May 1997) is in solar minimum phase. The ambient solar wind speed lower than 400 km/s. However, there's a major CME event on May 12th and high speed solar wind ejecta around May 15th. We use the full rotation synoptic chart as input, and optimized the parameters in the empirical function for the last 5 rotations preceding it (as regard to MSE). We do so as to observe the best performance of each model while keeping a certain level of objectivity.

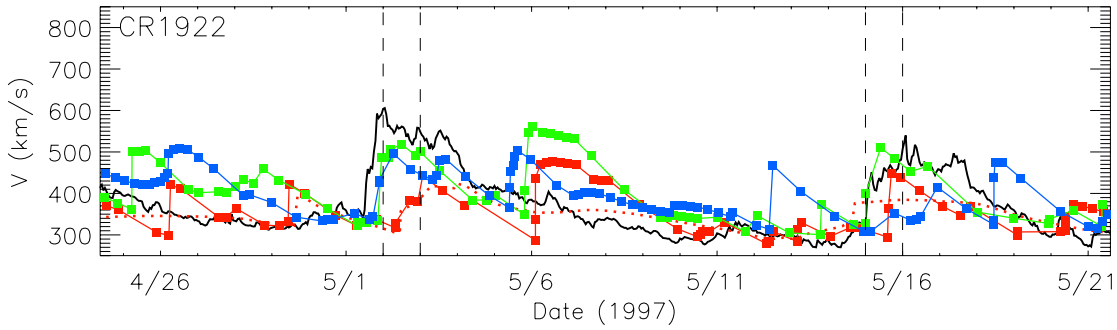

Fig5 Predicted solar wind speed during CR1922 (MDI, od22).

Red: PFSS; Green: SCS; Blue: HCCSSS; Red dotted: old WSA model; Black: WIND observed speed

Overall, all three models have improved a lot from the original WSA model (red dotted line) which does not include θ_b. SCS captures both two high speed events during this rotation, one around May 2nd and one around May 15th. PFSS misses the first one; HCCSSS misses the second. While all three models predict some slow solar winds accurately, they mistakenly report high speed events as well (April 27th and May 6th for all three models; May 13th and May 19th for HCCSSS).

During the solar minimum, the sub-earth line is constantly near the current sheet, where the expansion factors are huge. This correctly leads to low speed solar winds. However, in this period, the result becomes sensitive to the accuracy of field line tracing scheme, since a small deviation of the foot point location can result in a significant change of the expansion factor. Different field configurations of three models (fig2) naturally lead to different predictions.

We are able to make the global wind speed prediction near the sun as well (fig6). By tracing the field lines downward from the sub-earth point, we can find the origins of the solar wind materials. It is

apparent that HCCSSS reproduces a much more uniform speed distribution. The explanation is as following. As the polar field in HCCSSS extends to the lower latitude, the fluxes at are redistributed, with the original weak low latitude field (at 2.5$R_{\odot}$) increases in strength, and the polar field decreases. The expansion factors are then more evenly distributed, resulting in a more uniform distribution of speed. On the contrary, there are more variations of field strength in PFSS and SCS, and the polar fields are stronger. Thus, we get speed higher than 700 km/s constantly. Note that there is a north-south asymmetry in the global prediction. This also comes from our polar field correction.

The red lines in each map specify the origin of those two high speed events. Time runs from right to left. In out kinetic model, fast winds that are ejected later in time catch up with the previous slow ones. The fast ones then slow down. They push the slow ones in front of them, but never surpass them.

For the May 2nd event, All three models indicate that the source is from the extended part of the large coronal hole in the southern hemisphere. The existence of current sheet in SCS and HCCSSS model "draws" the field lines towards it, diminishes the areas with large expansion factors. Some the sub-earth points then reside out of this region in these two models and reproduce faster winds. These maps also show the sources of the May 15th event. They set out around May 12th, which is exactly the time of the CME event (Arge, 2003). This time the HCCSSS model gives larger expansion factors than the other two, which is consistent with its extensively expanded polar fields.

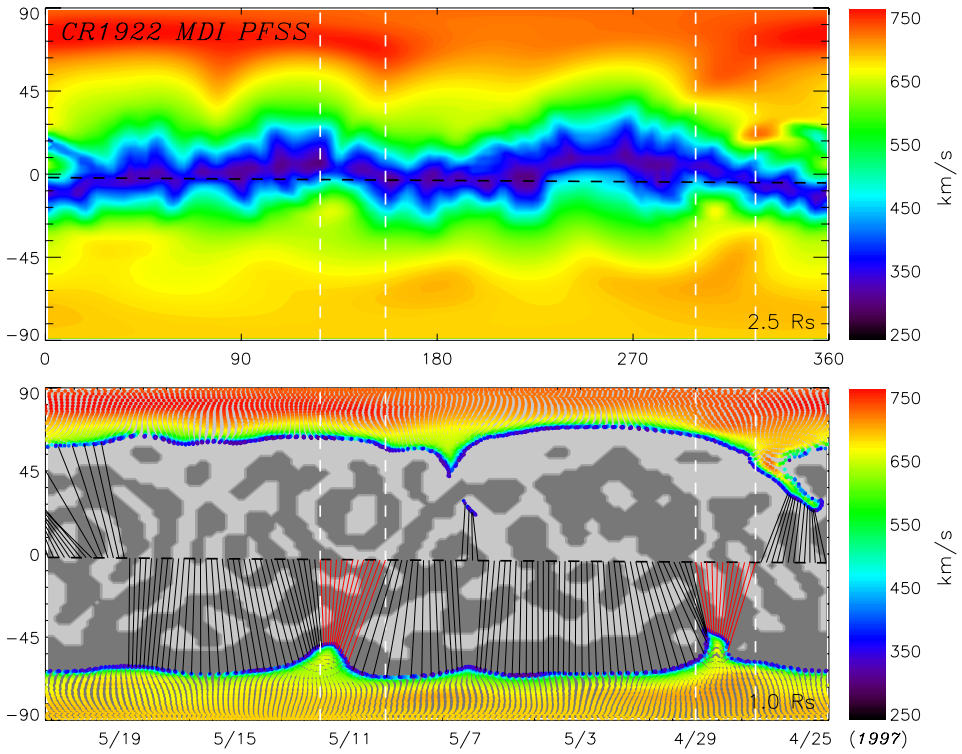

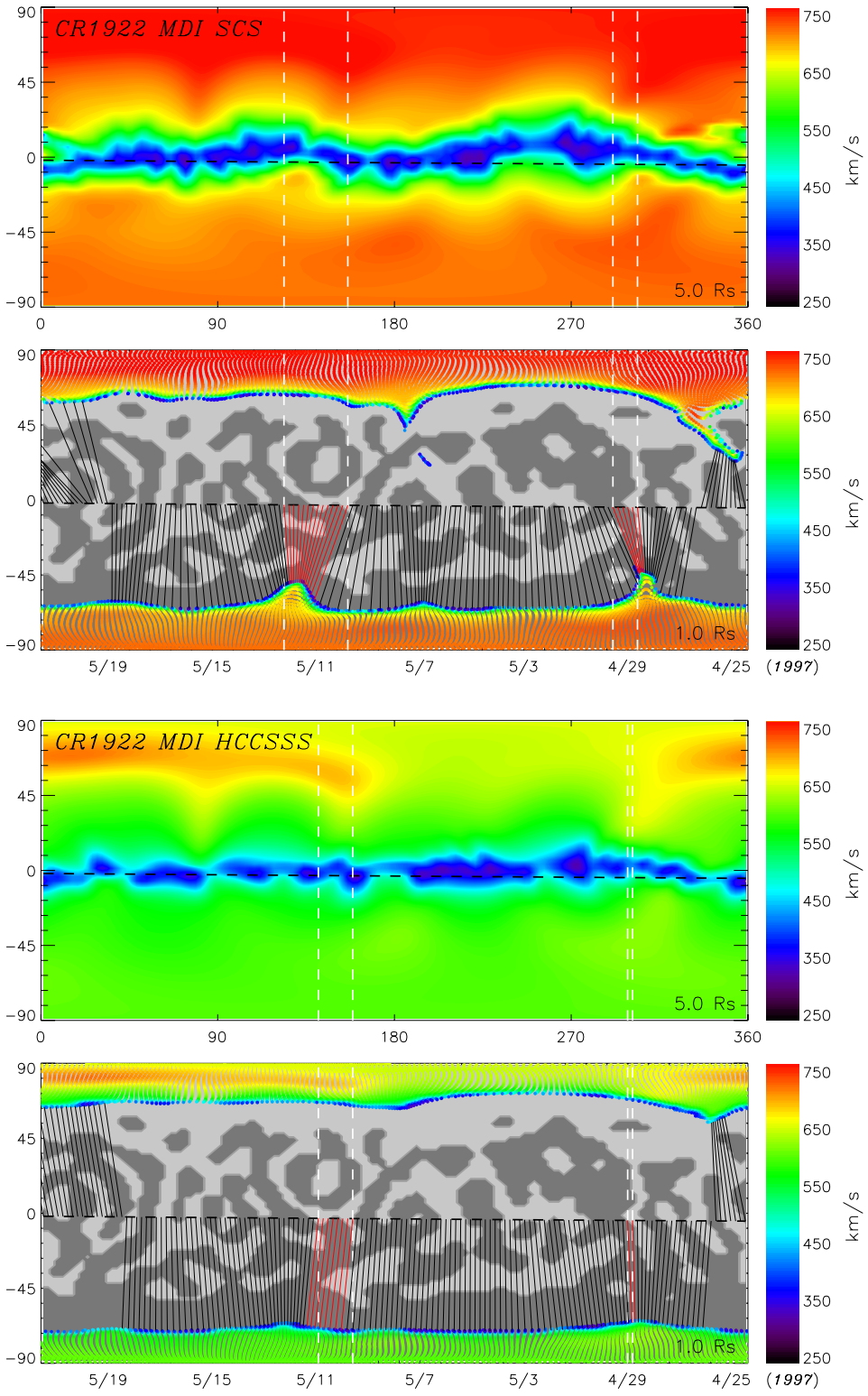

Fig6 Upper: PFSS; Middle: SCS; Lower: HCCSSS (CR1922, MDI, order22)

In each pane, Upper: global speed prediction; Lower: foot points with speed specified, reconstructed photospheric field polarity (light for positive, dark for negative), and sub-earth point connectivity to the photosphere.

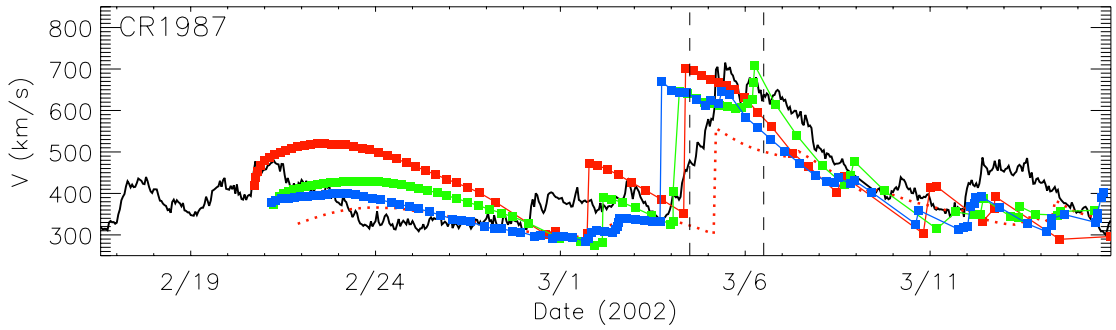

Fig7 Same as fig5, for CR1987 (MDI, od22).

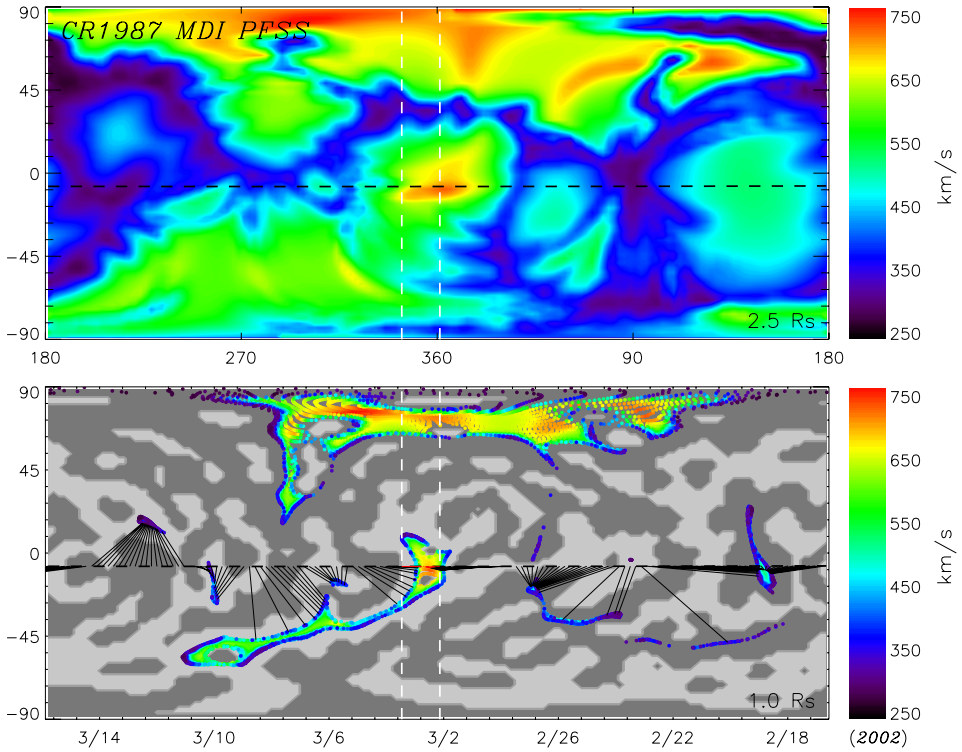

Fig8 Same as fig6, for PFSS CR1987

Carrington rotation 1987 (March 2002) gives an example of how these models work around solar maximum. There is a high speed event (fig7) at the beginning of this rotation. We take a synoptic map centered at Carrington longitude 360º to avoid the numerical effect on the edge. All three models successfully reproduce this event. Again, HCCSSS displays a more uniform speed distribution. At this

phase of solar cycle, the open flux areas and the total absolute open flux become smaller than the solar minimum. However, the current sheet reaches high latitude, so the expansion factors becomes highly variable along the sub-earth line. An interesting characteristic about this high speed event, as seen from all three models, is that it originates from a open field area near the equator. Field lines are almost radial-like in the lower corona.

Comparison of Predictions over a Solar Cycle

Making predictions over the whole solar cycle allows us to observe the performance of three models on a large time scale. Our expectation is to discover systematic characteristics inherent to each model. For example, how the parameters in the empirical function changes with time, or if one model always performs better than the other.

The first step is the comparison of the essential parameters: f_s and θ_b. The expansion factors of HCCSSS are generally smaller and more uniform than those of SCS and PFSS, as we explain above. It gives a clearer inverse relationship between the expansion factor and the speed at certain time period, for example, June 2003 to June 2005, but not so much during the others (fig9). The angular distance θ_b generally falls in the range of 2º to 4º. It corresponds to the solar wind speed very well.

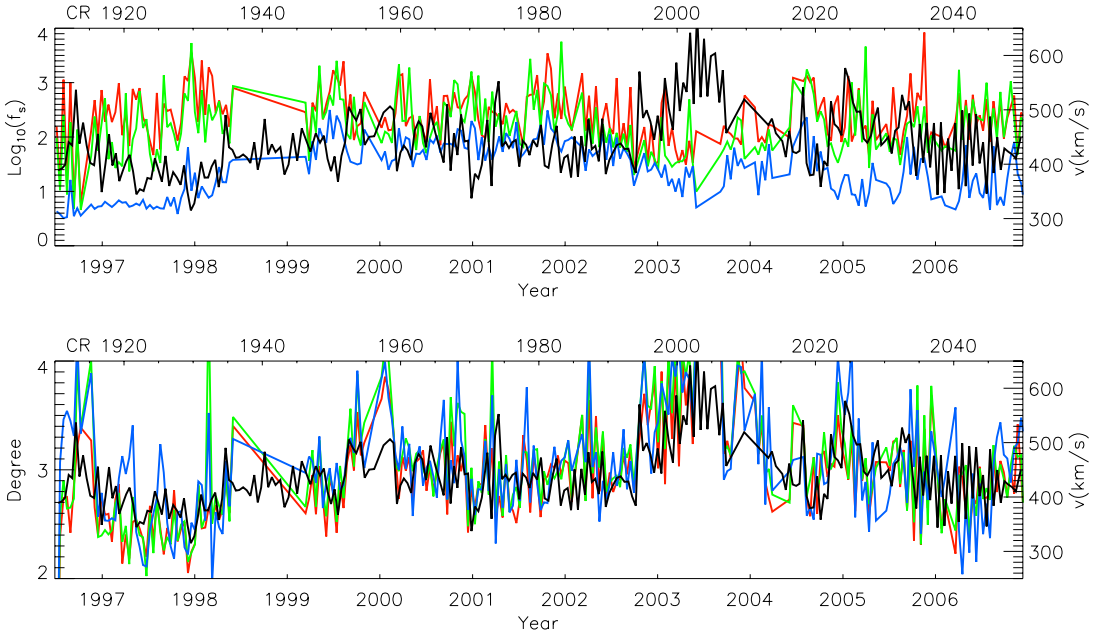

Fig9 Upper: f_s over the solar cycle; Lower: θ_b over the solar cycle.

Red: PFSS; Green: SCS; Blue: HCCSSS; Black: WIND speed

Fig9 again validates the empirical function used for WSA. However, it also points out that this relation could be extremely model dependent. While PFSS and SCS are more similar to each other, the HCCSSS gives a much smaller expansion factor. If an optimized function for SCS is found, its exponential on the $(1+f_s)$ part must be increased for the use of HCCSSS.

Keeping the characteristic angular distance θ_b (2.5º) and the highest possible speed unchanged, we adjust other parameters in the empirical function to fit the WIND proton speed data. Data with low temperature are excluded, and MSE is used as the criteria. After searching over the parameter space, we adopt one single parameter set for each model that has the minimum overall MSE over the solar cycle. We then apply this set of parameters to the prediction over 8 years (fig10).

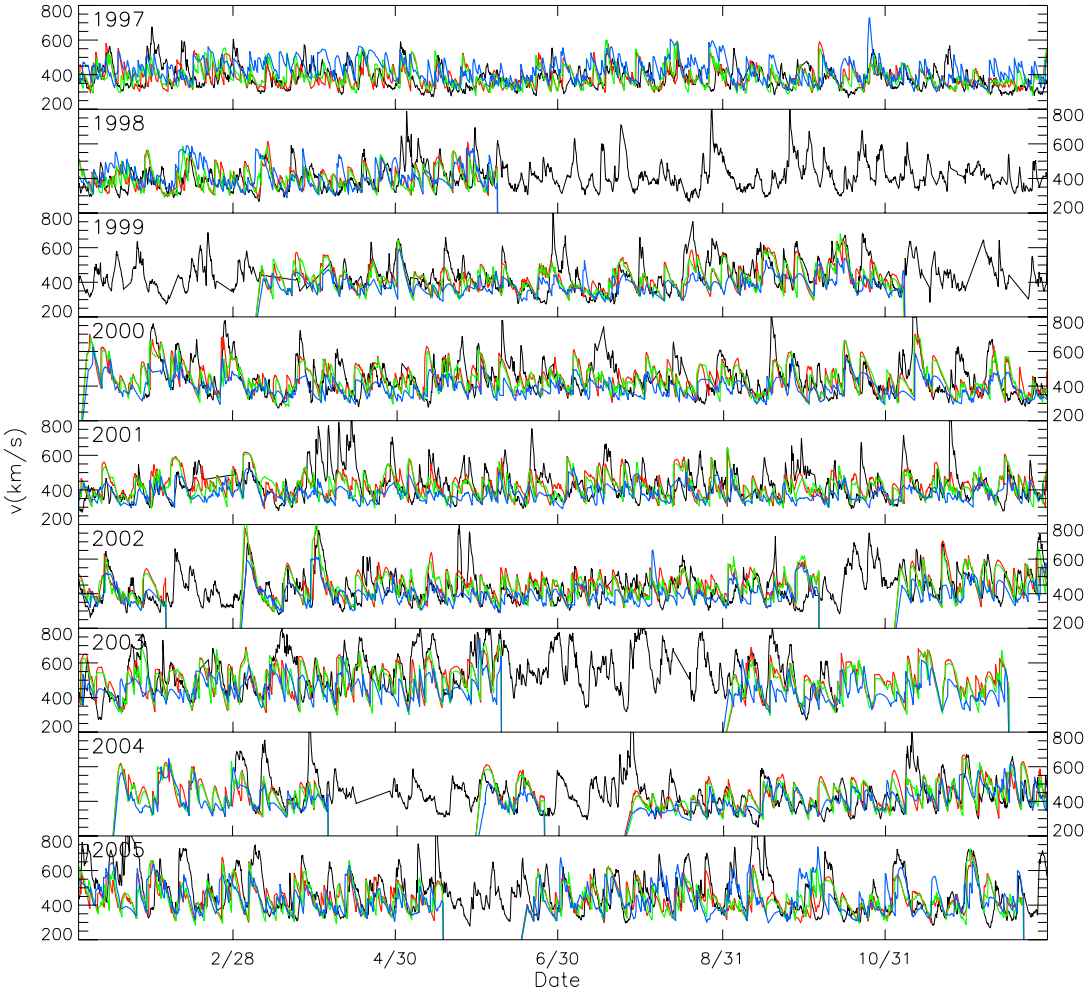

Fig10 Prediction of solar wind from 1998 to 2005.

Red: PFSS; Green: SCS; Blue: HCCSSS; Black: WIND speed

Ambient solar wind speed is not necessary the slowest during minimum and the fastest during

maximum. Rather, fast solar wind are the most frequently observed in 2003 during this 8 year period, almost 2 years behind the solar maximum. On the other hand, the area of open flux regions follows an inverse relationship with the solar cycle more strictly (fig4).

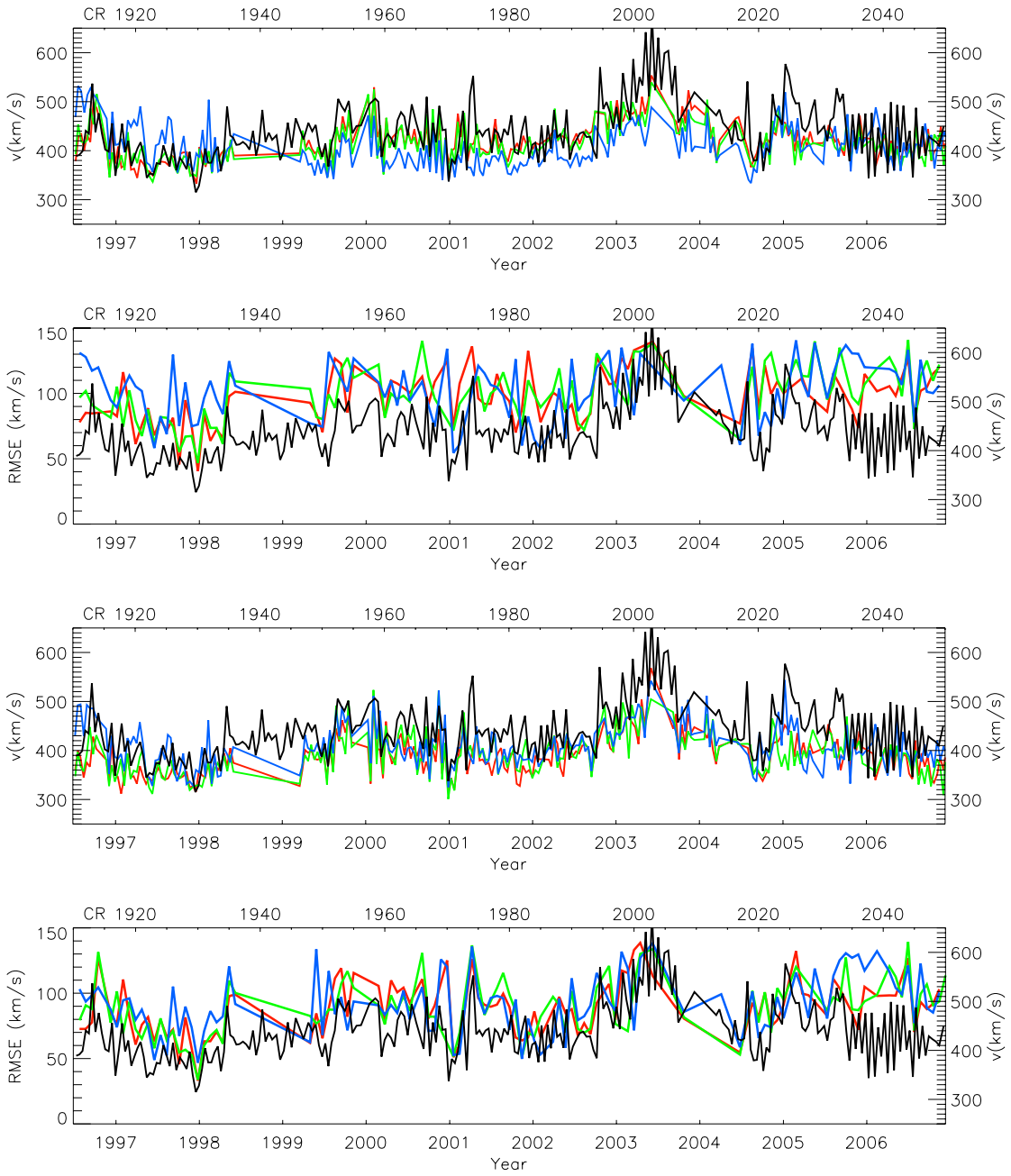

Fig 11 Predicted solar wind speed and RMSE from CR1911 to CR2050.

Red: PFSS; Green: SCS; Blue: HCCSSS; Black: WIND speed

Top 2: With single set of parameter over the whole period; Bottom 2: With best fitted parameters rotation by rotation.

The single empirical function in this 8 year period leads to a systematic difference between three models. While HCCSSS constantly predicts higher speed than PFSS and SCS during 1997, its prediction is constantly lower from 2000 to 2003. In 2005, its prediction is comparable to the other two again (fig11a). In this case, the MSE is more uniform through out the whole period, for all three models, which means a higher relative deviation during the solar minimum (fig11b).

A biased approach, i.e. optimizing the empirical function rotation by rotation, allows us to study the limit of these models. In this sense, all three models work similarly during the whole time period, without apparent systematic differences (fig11c). The MSE now varies according to the averaged ambient wind speed (fig11d), so the relative errors are more uniform through out these 8 years. Year 2006 is an exception. Since the polar field are now the extrapolated ones rather than the interpolated ones, we suspect this correction is the major source of errors.

Fig11 shows that: (1) if only one set of parameter is allowed in the empirical function, SCS generally works better than HCCSSS. Since SCS has the same filed configuration as PFSS below $2.5R_{\odot}$ and better one above it, it is the best amongst the three. (2) If we could find an "idealized" function that's objectively varies with time, or at most depends on the modeled field itself, there could be no inherent difference to these three models.

Discussion of Miscellaneous Issues:

1. Polar Field Correction

   Polar field correction is essential to obtaining a reasonable coronal field structure. Unreasonable polar field will lead to misplaced foot point locations, and eventually inaccurate predictions (fig11).

   We take those well observed MDI polar data (September for north pole and March for south pole). For each specific point in the polar region, we get a time series of field values over ten years. A cubic-spline fit is used to determine the value at each specific time (Liu, 2007). This method proves to be the best among the common polar corrections (fig12).

   This method is largely successful at reproducing the foot points configurations, but the north-south polar fields are usually asymmetric (fig12). After taking out the monopole component, the global field magnitude zero-point might shift, causing the shift or deformation of the current sheet. During the solar minimum, this shift of current sheet towards the sub-earth line could result in too uniform and huge expansion factors, thus too low speeds with little variation.

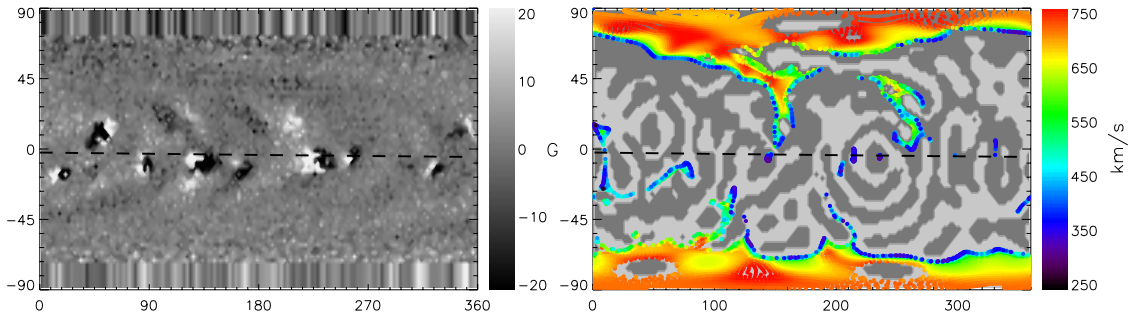

Fig11 Artificial polar field correction and its effect on foot point locations (CR2029, PFSS, MDI).

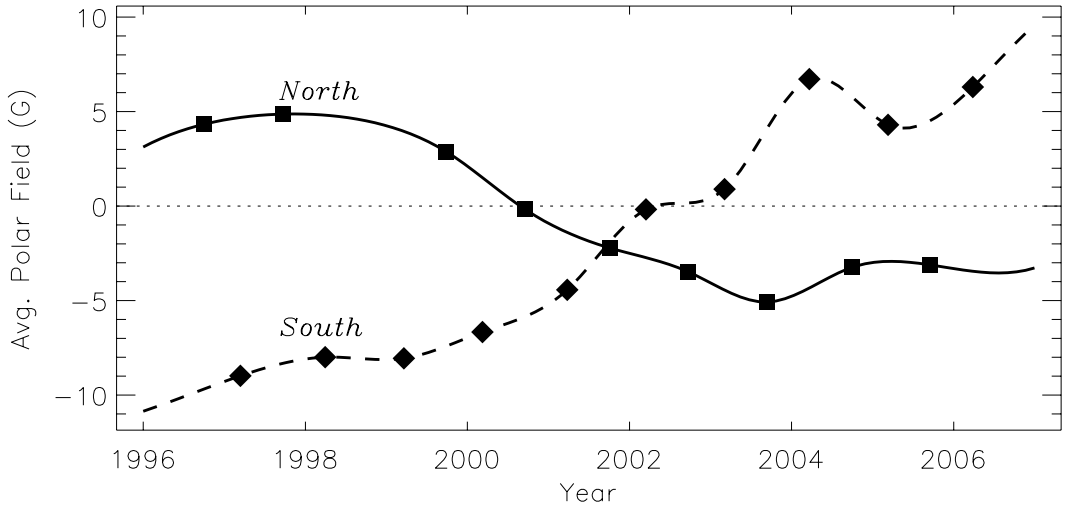

Fig12 Mean field of reconstructed MDI polar data, cubic-spline-fitted.

2. Input Data Format: sine latitude or latitude

In the sine latitude format synoptic chart, each grid cell has the same area, so the flux is proportional to the observed field value. However, fields above certain latitude are not resolved. (For example, the WSO data has a -14.5/15~14.5/15 sine latitude grid. The highest cell center is located at 75.2º, above which we have no data.)

As we compute the harmonic coefficient for the potential field, the numerical effect becomes serious. If we use sine latitude format, the numerical integral algorithm emphasizes too much on the polar fields. Furthermore, the eigenvectors in sine latitude format are not orthogonal with each other, causing unrealistic fluctuations in field magnitude (fig13).

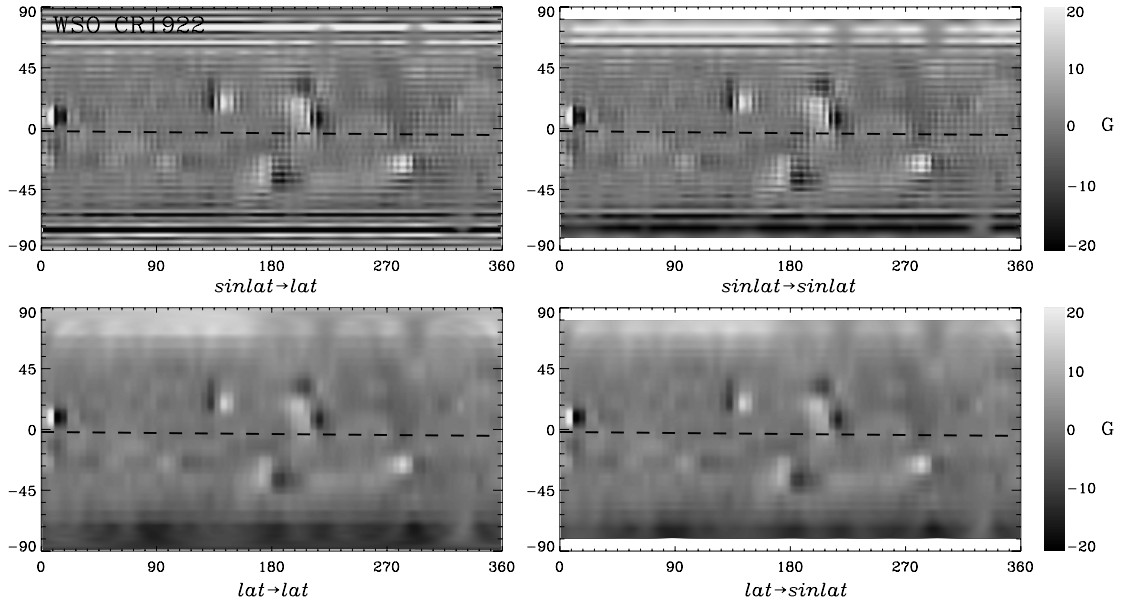

Fig13 Reconstructed synoptic chart with various input/output format (CR1922, WSO, PFSS, order 22)

Upper-left: sin-lat input, lat output; Upper-right: sin-lat input, sin-lat output;

Lower-left: lat input, lat output; Lower-right: lat input, sin-lat output.

3. Effect of N_{max}

The maximum order of harmonic coefficient is important when computing the field. Past study (Bala and Zhao, 2004) shows that for PFSS model and WSO data, N_{max}=22 seems to be a reasonable choice. By mapping back from 1AU to $1R_{\odot}$, solar wind speed are connected with the single parameter f_s. Above order 22, the locations of certain foot points and the computed expansion factors become stable.

We make the global speed prediction with different orders of harmonic coefficient (fig14). Compare this with fig6, we see the foot point locations are similar for order 22 and 72, while order 9 oversimplifies the configurations. Also, we find the predicted speed is too low for order 9. For order 72, the prediction introduces some artificial fluctuation in speed, as well as lots of local mixed polarities, both of which are possibly due to numerical effects. According to the limited cases we have explored, order 22 already gives a relatively smooth distribution of speed and photospheric field, and the predictions at 1AU are no worse then higher order computations. We argue that order 22 is the most reasonable choice amongst the three.

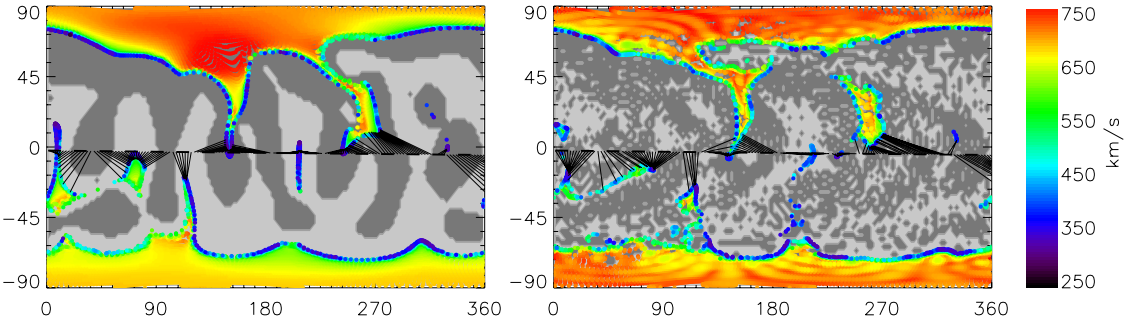

Fig14 Foot points location and photospheric field (CR2029, PFSS, MDI).

Left: order 9; Right: order 72.

Conclusion and Challenges:

In the hope to improve the WSA model, we explore various possible approaches. For the input data, a temporal interpolation is used for polar correction, and latitude grid format is adopted. For the prediction algorithm, the parameter θ_b greatly improves the prediction.

We also make a preliminary comparison between three models. The HCCSSS model gives a different field configuration than the other two, with a more expanded polar field. Thus, it predicts a more uniform solar wind prediction. A rotation by rotation optimization of the empirical function shows the limit of three models, and there's no inherent difference between three models if the empirical function can be "objectively optimized". However, by using a single best fitted empirical function over 8 years of time, we demonstrate that SCS model generally performs better amongst the three.

Several questions remain unsolved:

1. The temporal interpolation introduces a north-south asymmetry, whose effects are still unknown.
2. The HCCSSS model fixes the kinks of field lines at $2.5R_\odot$, satisfies the magneto-static equation, so it seems to be the best amongst the three. However, since it relaxes the radial constraint at $2.5R_\odot$, it does not do a good job at evaluation the field strength. Whether this radial constraint is essential here is really worth studying.
3. An appropriate statistical evaluation that could guide this study is to be found.
4. The predictions are sensitive to the free parameters in the empirical function. Finding a robust yet objective function so that the model could reach its limit will be our next step.

References:

Wang, Y.-M. & Sheeley Jr., N. R., 1990, ApJ, 355, 726.

Arge, C. N. et al., 2003, Solar Wind Ten, CP679.

Schatten, K. H., 1971, Cosmic Electrodynamics, 2, 232.

Zhao, X. & Hoeksema, T., 1994, Solar Physics, 151, 91.

Bala, P. & Zhao, X., 2004, J. Geo. Res., 109, A08102.

Richardson, I. G. & Cane, H. V., 1995, J. Geo. Res., 100, 23297